Computing the propagation characteristics of radially stratified fibers: an efficient method

C. Yeh and G. Lindgren

An efficient method is introduced in this paper to compute the dispersion characteristics as well as the Poynting flux distribution of radially stratified fibers. Only 4 × 4 matrix operations were needed. Detailed results are given for several representative radially inhomogeneous fibers of practical interest.

I. Introduction

It has become increasingly clear that radially inhomogeneous fibers must be used to maximize the information carrying capacities of the optical fiber transmission system. Efficient analytical means must be found to predict the propagation characteristics of various modes in such inhomogeneous fibers. It is known that unlike the homogeneous fiber case, the wave equation governing the fields for radially inhomogeneous fibers consists of two coupled second-order differential equations whose solutions are usually very difficult to obtain. Using the numerical integration technique, Dil and Blok[1] and later Vassell[1] solved these equations for a fiber with radial parabolic dielectric profile. Yip and Ahmew,[2] using the same technique, solved the problem of a cladded fiber with a radial parabolic index profile. However, this method of solution is very time consuming, hence very expensive. Furthermore to achieve computational efficiency, their consideration is restricted to the square law distribution of permittivity wherein a power series expansion may be used to represent the field variation as a function of the radial coordinate.

A useful approximate approach for an analytical solution of electromagnetic problems involving a radially inhomogeneous column is to subdivide it into thin homogeneous layers and to solve an easier problem in each layer. The fields in each layer are expanded in appropriate eigenfunctions and the expansion coefficients determined by matching boundary conditions. However, this straightforward approach becomes much too tedious, and the number of simultaneous equations to be solved tends to be prohibitively large as the number of layers increases.[3] Using this technique, the number of layers that may be used is quickly limited by the capacity of a modern computer. It is therefore quite apparent that a different approach must be taken. The purpose of the present investigation is to seek a simple way to solve the problem of guided waves in inhomogeneous fibers without the forementioned difficulties and limitations. (Exhaustive comparison with other techniques in terms of computer time is not possible or warranted, but typically the computer time requirement for the present technique using five layers is three times less than that used in Ref. 3 and ten times less than that used in Refs. 1 and 2.) We shall show that by appropriately manipulating the simultaneous equations obtained according to the homogeneous layers approach, we shall only deal with 4 × 4 type matrix operations. Hence the constraint on the number of layers used to approximate the inhomogeneous profiles can be eliminated. Furthermore, the required results can be obtained very quickly (efficient usage of computer time) with this technique. We shall apply this method to determine the dispersion characteristics and the Poynting flux distribution of several radially inhomogeneous fibers of practical interests.

II. Formulation of the Problem

Without loss of generality we may assume that the expressions for the field components of all modes are multiplied by the factor $\exp(in\theta + i\beta z - i\omega t)$, which will be suppressed throughout.

Dividing the fiber guide into $m + 1$ region, as shown in Fig. 1, we may write the expressions for the tangential fields in these regions as follows:
in region 1,

$$\begin{bmatrix} E_z^{(1)} \\ \eta H_z^{(1)} \\ \rho E_\theta^{(1)} \\ \eta\rho H_\theta^{(1)} \end{bmatrix} = \begin{bmatrix} c_1(r) & 0 & 0 & 0 \\ 0 & d_1(r) & 0 & 0 \\ e_1(r) & f_1(r) & 0 & 0 \\ q_1(r) & h_1(r) & 0 & 0 \end{bmatrix} \begin{bmatrix} C_1 \\ D_1 \\ 0 \\ 0 \end{bmatrix}; \quad (1)$$

in region $m (m > 1)$,

When this work was done both authors were with University of California, Electrical Science & Engineering Department, Los Angeles, California 90024. G. Lindgren is now with Hughes Aircraft Company, Canoga Park, California 00000.

Received 27 February 1976.

$$\begin{bmatrix} E_z^{(m)} \\ \eta H_z^{(m)} \\ \rho E_\theta^{(m)} \\ \eta\rho H_\theta^{(m)} \end{bmatrix} = \begin{bmatrix} c_m(r) & 0 & c_m'(r) & 0 \\ 0 & d_m(r) & 0 & d_m'(r) \\ e_m(r) & f_m(r) & e_m'(r) & f_m'(r) \\ g_m(r) & h_m(r) & g_m'(r) & h_m'(r) \end{bmatrix} \begin{bmatrix} C_m \\ D_m \\ C_m' \\ D_m' \end{bmatrix}; \quad (2)$$

in region $m+1$ (the outermost region),

and $C_1, D_1, \ldots, C_m, D_m, C_m', D_m' \ldots G, F$ are arbitrary constants. It has been assumed that within each region the permittivity is a constant.

Matching the tangential electric and magnetic fields at the bounding surfaces, i.e., $r = r_1, r_2, \ldots r_m$ (see Fig. 1), gives

$$\begin{bmatrix} c_1 & 0 & 0 & 0 \\ 0 & 0 & d_1 & 0 \\ e_1 & 0 & f_1 & 0 \\ g_1 & 0 & h_1 & 0 \end{bmatrix} \begin{bmatrix} C_1 \\ 0 \\ D_1 \\ 0 \end{bmatrix} = \begin{bmatrix} c_2 & c_2' & 0 & 0 \\ 0 & 0 & d_2 & d_2' \\ e_2 & e_2' & f_2 & f_2' \\ g_2 & g_2' & h_2 & h_2' \end{bmatrix} \begin{bmatrix} C_2 \\ C_2' \\ D_2 \\ D_2' \end{bmatrix}$$

$$\begin{bmatrix} c_2 & c_2' & 0 & 0 \\ 0 & 0 & d_2 & d_2' \\ e_2 & e_2' & f_2 & f_2' \\ g_2 & g_2' & h_2 & h_2' \end{bmatrix} \begin{bmatrix} C_2 \\ C_2' \\ D_2 \\ D_2' \end{bmatrix} = \begin{bmatrix} c_3 & c_3' & 0 & 0 \\ 0 & 0 & d_3 & d_3' \\ e_3 & e_3' & f_3 & f_3' \\ g_3 & g_3' & h_3 & h_3' \end{bmatrix} \begin{bmatrix} C_3 \\ C_3' \\ D_3 \\ D_3' \end{bmatrix}$$

$$\begin{bmatrix} c_{m-1} & c_{m-1}' & 0 & 0 \\ 0 & 0 & d_{m-1} & d_{m-1}' \\ e_{m-1} & e_{m-1}' & f_{m-1} & f_{m-1}' \\ g_{m-1} & g_{m-1}' & h_{m-1} & h_{m-1}' \end{bmatrix} \begin{bmatrix} C_{m-1} \\ C_{m-1}' \\ D_{m-1} \\ D_{m-1}' \end{bmatrix} = \begin{bmatrix} c_m & c_m' & 0 & 0 \\ 0 & 0 & d_m & d_m' \\ e_m & e_m' & f_m & f_m' \\ g_m & g_m' & h_m & h_m' \end{bmatrix} \begin{bmatrix} C_m \\ C_m' \\ D_m \\ D_m' \end{bmatrix}$$

$$\begin{bmatrix} c_m & c_m' & 0 & 0 \\ 0 & 0 & d_m & d_m' \\ e_m & e_m' & f_m & f_m' \\ g_m & g_m' & h_m & h_m' \end{bmatrix} \begin{bmatrix} C_m \\ C_m' \\ D_m \\ D_m' \end{bmatrix} = \begin{bmatrix} s & 0 & 0 & 0 \\ 0 & 0 & \tau & 0 \\ u & 0 & v & 0 \\ w & 0 & \chi & 0 \end{bmatrix} \begin{bmatrix} E \\ 0 \\ F \\ 0 \end{bmatrix}, \quad (5)$$

$$\begin{bmatrix} E_z^{(m+1)} \\ \eta H_z^{(m+1)} \\ \rho E_\theta^{(m+1)} \\ \eta\rho H_\theta^{(m+1)} \end{bmatrix} = \begin{bmatrix} 0 & 0 & s(r) & 0 \\ 0 & 0 & 0 & \tau(r) \\ 0 & 0 & u(r) & v(r) \\ 0 & 0 & w(r) & \chi(r) \end{bmatrix} \begin{bmatrix} 0 \\ 0 \\ G \\ F \end{bmatrix}; \quad (3)$$

where

$$c_m(r) = J_n(p_m r), \qquad c_m'(r) = N_n(p_m r),$$

$$d_m(r) = iJ_n(p_m r), \qquad d_m'(r) = N_n(p_m r)i,$$

$$e_m(r) = -\frac{\beta n k_0}{p_m^2} J_n(p_m r), \qquad e_m'(r) = -\frac{\beta n k_0}{p_m^2} N_n(p_m r),$$

$$f_m(r) = -\frac{ik_0}{p_m} k_0 r J_n'(p_m r)i, \qquad f_m'(r) = \frac{-ik_0}{p_m} k_0 r N_n'(p_m r)i,$$

$$g_m(r) = i\frac{\epsilon_m}{\epsilon_0}\frac{k_0}{p_m} k_0 r J_n'(p_m r), \qquad g_m'(r) = \frac{\epsilon_m}{\epsilon_0}\frac{k_0}{p_m} k_0 r N_n'(p_m r),$$

$$h_m(r) = -\frac{n\beta k_0}{p_m^2} \times J_n(pr)i \qquad h_m'(r) = \frac{-n\beta k_0}{p_m} N_n(p_m r)i,$$

$$s(r) = K_n(qr),$$

$$\tau(r) = K_n(qr),$$

$$u(r) = \frac{\beta n k_0}{q^2} K_n(qr),$$

$$v(r) = \frac{ik_0}{q} k_0 r K_n'(qr)i,$$

$$w(r) = -i\frac{\epsilon_{m+1}}{\epsilon_0}\frac{k_0}{q} \times k_0 r K_n'(qr),$$

$$\chi(r) = \frac{\beta n k_0}{q^2} K_n(qr)i,$$

$$p_m^2 = \omega^2\mu_0\epsilon_m - \beta^2,$$

$$k_m^2 = \omega^2\mu_0\epsilon_m, \qquad k_0 = \omega(\mu_0\epsilon_0)^{1/2},$$

$$q^2 = \beta^2 - \omega^2\mu_0\epsilon_{m+1}, \qquad \eta = [(\mu_0)/(\epsilon_0)]^{1/2}, \quad (4)$$

where the bar signifies that the functions $\boldsymbol{c}_n, \boldsymbol{c}_n' \ldots \boldsymbol{h}_n, \boldsymbol{h}_n'$ are evaluated at the surface $r = r_n$. The functions $c_n, c_n' \ldots h_n, h_n'$ are evaluated at the surface $r = r_{n-1}$. It is clear that if one sets the determinant of the above simultaneous equations to zero, one obtains in a straightforward manner the dispersion relation for the inhomogeneous fiber problem. However, one notes that the size of the resultant determinant depends directly on the number of layers that we use. The unattractive numerical problems associated with a very large size matrix are well known. Fortunately, for the inhomogeneous fiber problem, a way can be found to avoid working with this large-size matrix.

Realizing the fact that we may express the array

$$\begin{bmatrix} C_2 \\ C_2 \\ D_2 \\ D_2' \end{bmatrix}$$

in terms of

$$\begin{bmatrix} C_3 \\ C_3' \\ D_3 \\ D_3' \end{bmatrix}$$

etc., one may write down the following chain equation:

$$\mathbf{M}_1 \begin{bmatrix} C_1 \\ 0 \\ D_1 \\ 0 \end{bmatrix} = M_2\mathbf{M}_2^{-1}M_3\mathbf{M}_3^{-1} \ldots M_m\mathbf{M}_m^{-1}M_{m+1} \begin{bmatrix} E \\ 0 \\ F \\ 0 \end{bmatrix}, \quad (6)$$

where

$$M_1 = \begin{bmatrix} c_1 & 0 & 0 & 0 \\ 0 & 0 & d_1 & 0 \\ e_1 & 0 & f_1 & 0 \\ g_1 & — & h_1 & 0 \end{bmatrix},$$

$$M_m = \begin{bmatrix} c_m & c_m' & 0 & 0 \\ 0 & 0 & d_m & d_m' \\ e_m & e_m' & f_m & f_m' \\ g_m & g_m' & h_m & h_m' \end{bmatrix},$$

$$M_m^{-1} = \begin{bmatrix} c_m & c_m' & 0 & 0 \\ 0 & 0 & d_m & d_m' \\ e_m' & e_m' & f_m & f_m' \\ g_m & g_m' & h_m & h_m' \end{bmatrix}^{-1},$$

$$M_{m+1} = \begin{bmatrix} s & 0 & 0 & 0 \\ 0 & 0 & \tau & 0 \\ u & 0 & v & 0 \\ w & 0 & \chi & 0 \end{bmatrix}.$$

Hence, we are now only dealing with matrix of size 4 × 4. This rearrangement eliminates the need to compute large matrix. The size of our present matrix is independent of the number of layers that we use. Hence, we may use as many layers as we wish to achieve the desired accuracy. Rewriting Eq. (6) gives

$$\begin{bmatrix} c_1 & 0 & -M_{11} & -M_{13} \\ 0 & d_1 & -M_{21} & -M_{23} \\ e_1 & f_1 & -M_{31} & -M_{33} \\ g_1 & h_1 & -M_{41} & -M_{43} \end{bmatrix} \begin{bmatrix} C_1 \\ D_1 \\ E \\ F \end{bmatrix} = 0, \qquad (7)$$

where M_{mn} are elements of the matrix M with

$$M = M_2 M_2^{-1} M_3 M_3^{-1} \ldots M_m M_m^{-1} M_{m+1}.$$

Setting the determinant of Eq. (7) to zero, one obtains the dispersion relation from which the propagation constants of various modes along an inhomogeneous fiber guide may be found. In other words, the propagation constants of various modes correspond to the roots of the dispersion relation. Given all known constants such as the frequency, the size of the fiber, the dielectric constant, thicknesses of the layers, etc., the roots can be found by the well-known Newton's method.

III. Numerical Results

The above technique is used to obtain the dispersion characteristics and Poynting flux distribution of several radially inhomogeneous fibers of practical interest. The refractive index profiles of these fibers are shown in Fig. 2. For the present computation, the refractive index is assumed to be independent of the frequency of operation. Figures 3 and 4 give, respectively, the normalized propagation constant $\beta_N = \beta/k_0$ vs the normalized frequency $k_0 a$ curves for several lower order modes of a homogeneous fiber and of an inhomogeneous with parabolic index variation. From a comparison of Fig. 3 to Fig. 4, one notices that the excursion of β/k_0 from the cutoff value to far above cutoff value occurs over a much larger range of $k_0 a$ when the profile is parabolic rather than homogeneous. This agrees with the minimal dispersion predictions provided by geometrical optics. The other interesting feature of the parabolic profile is that a number of the modes have merged or possess nearly degenerate dispersion curves.

The doughnut profile was studied in two forms, which are shown in Fig. 5. Figure 6 presents their respective dispersion diagrams. One notices from the curves that the dispersion is intermediate between the homogeneous core and the parabolic core and further that the mode merging is not complete. Profile (a) is less dispersive than (b) which follows since $\langle n \rangle_{nA}$ of (a) is less than that of (b).

Finally, the $HE_{1,1}$ mode dispersion characteristics of the three profiles (step, parabolic, and doughnut) are compared in Fig. 7. This shows that for a given radius and Δn, a guide is less dispersive as the profile departs from a step profile.

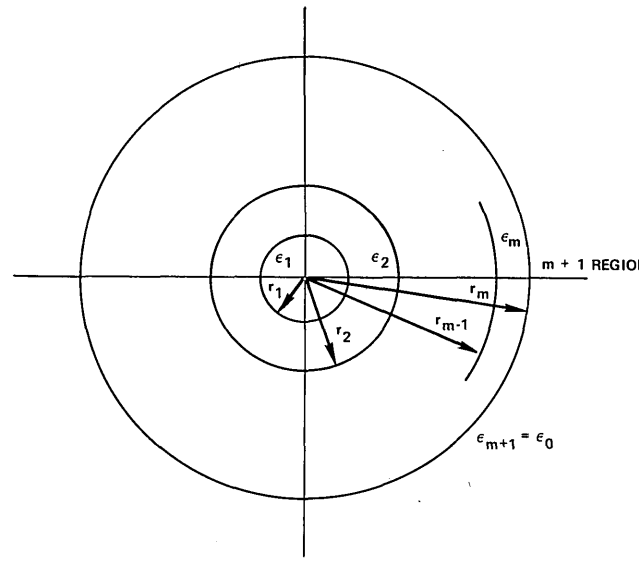

Fig. 1. Geometry of the inhomogeneous fiber.

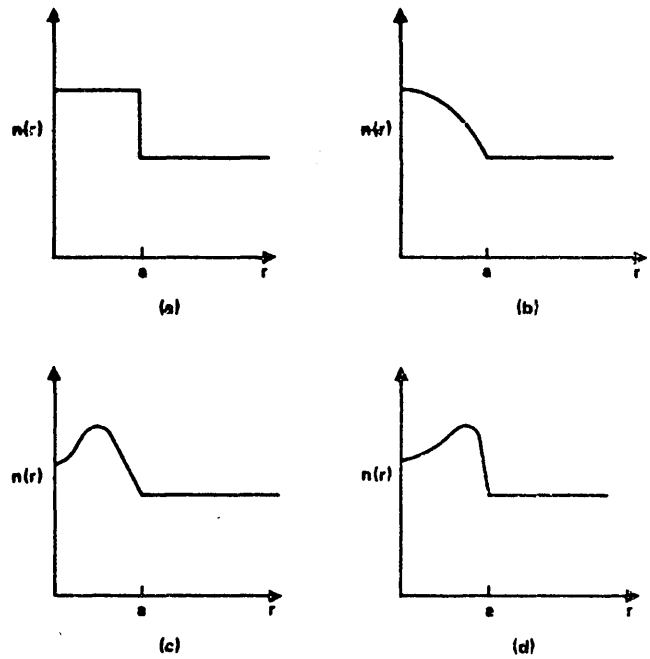

Fig. 2. Refractive-index profiles of several fibers of interest.

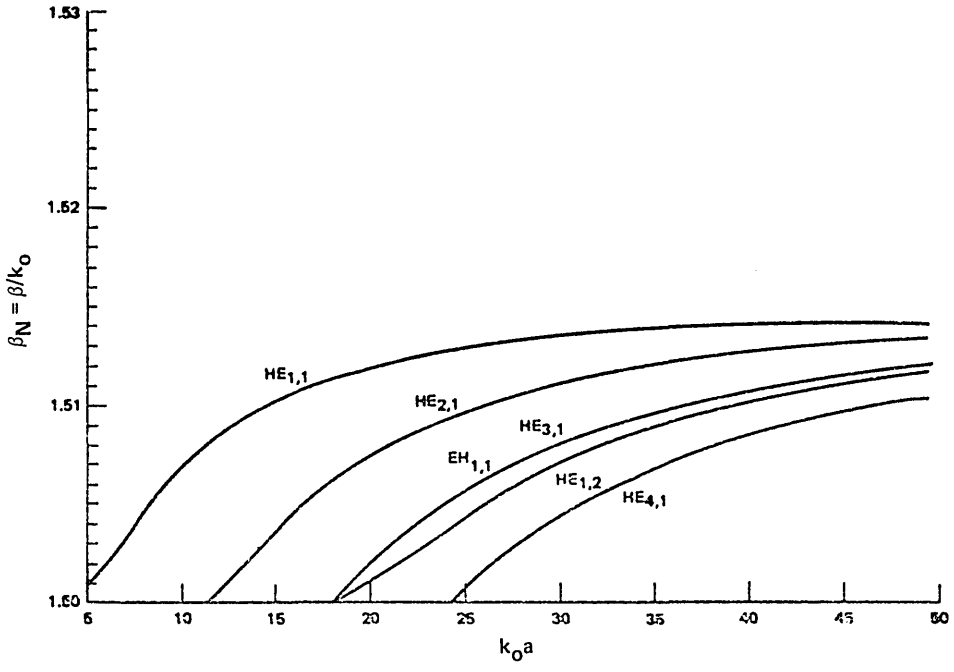

Fig. 3. Dispersion curves for homogeneous core fiber with n_1 = 1.515 and n_2 = 1.50. a is the radius of the core.

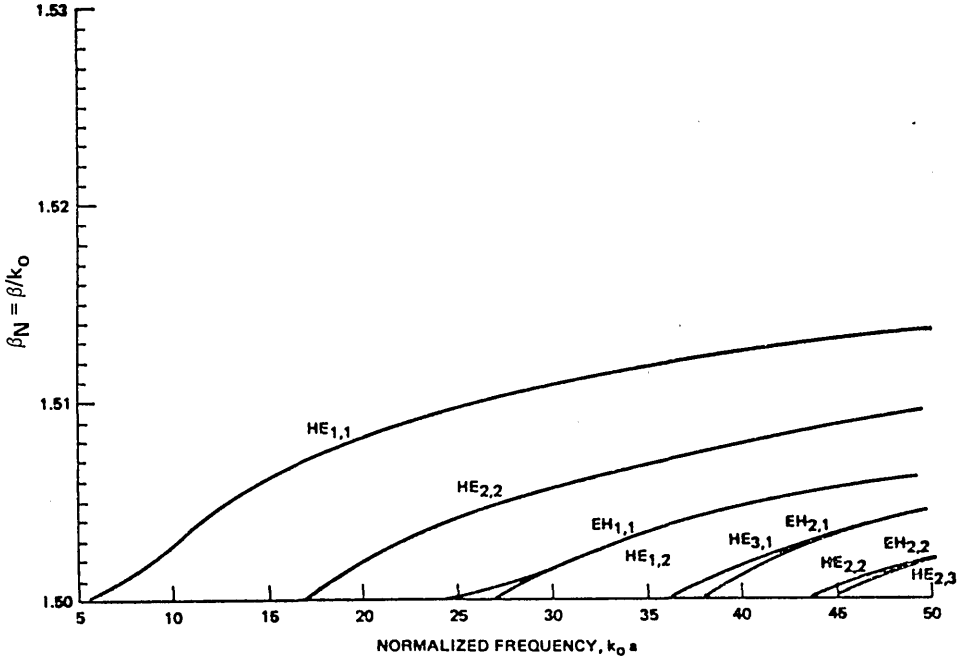

Fig. 4. Dispersion curves for parabolic core (five-layer) fiber with n_{MAX} = 1.515 and n_2 = 1.50.

The Poynting flux in the mth region of a fiber is given by

$$S_z(m) = \frac{1}{2}\,\mathrm{Re}\,[E_r(m)H\phi(m)^* - E_\phi(m)H_r(\mathrm{m})^*]. \quad (8)$$

The Poynting flux (energy density distribution) was computed for several representative profiles given in Fig. 2. The results are presented primarily at two operating conditions, near cutoff and far above cutoff, since the flux confinement is intermediate for other operating conditions.

Figures 8–12 show the behavior of some homogeneous core modes along with the percentage of power carried inside and outside the core region. The Poynting flux diagrams are shown throughout as normalized to the peak intensity of the flux and as a function of r along outward rays of peak intensity.

Upon examination of the Poynting flux diagrams, one will observe that the Poynting flux S_z has a slight discontinuity at $r = a$. This discontinuity arises simply because the E_r component of the field is not continuous across the boundary. Similarly, for the inhomogeneous core profiles, S_z is discontinuous at each stratification boundary. Figures 13 and 14 show S_z for the parabolic

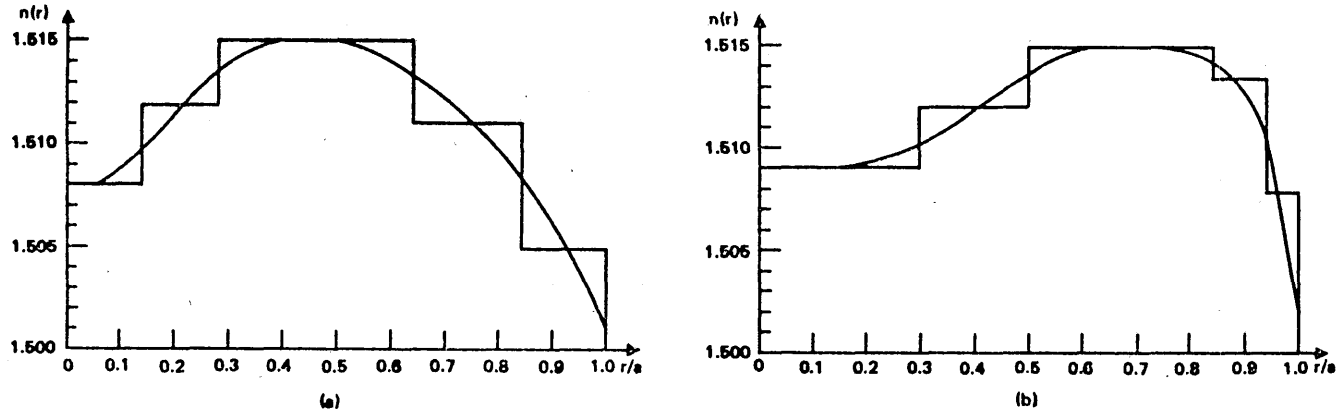

Fig. 5. Staircase approximations of two doughnut refractive-index profiles.

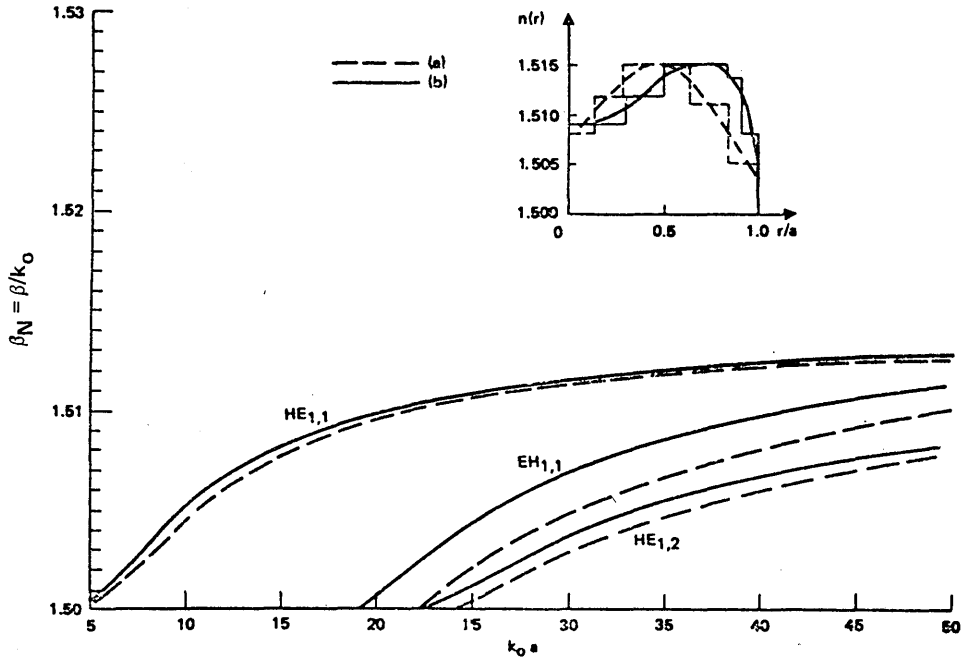

Fig. 6. Comparison of dispersion curves for two fibers with different doughnut refractive-index profiles.

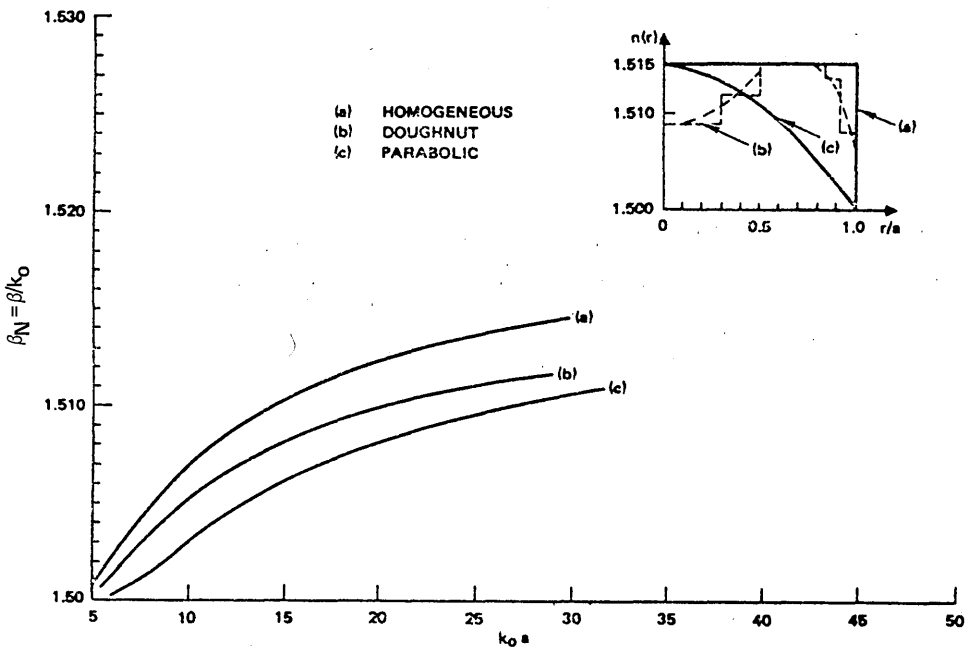

Fig. 7. Comparison of $HE_{1,1}$ mode dispersion curves for homogeneous, doughnut, and parabolic refractive-index profile fibers.

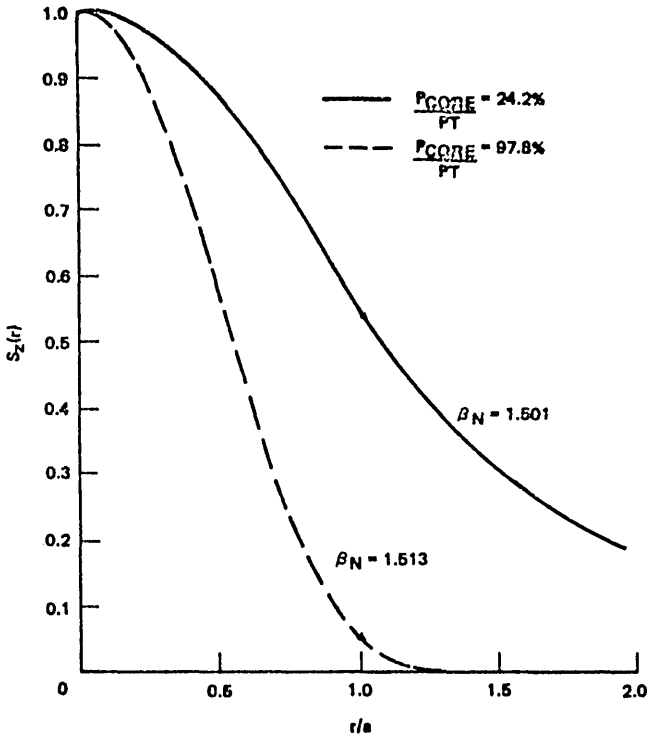

Fig. 8. Poynting flux characteristics of $HE_{1,1}$ mode. Fiber profile is homogeneous, $n_1 = 1.515$ and $n_2 = 1.500$.

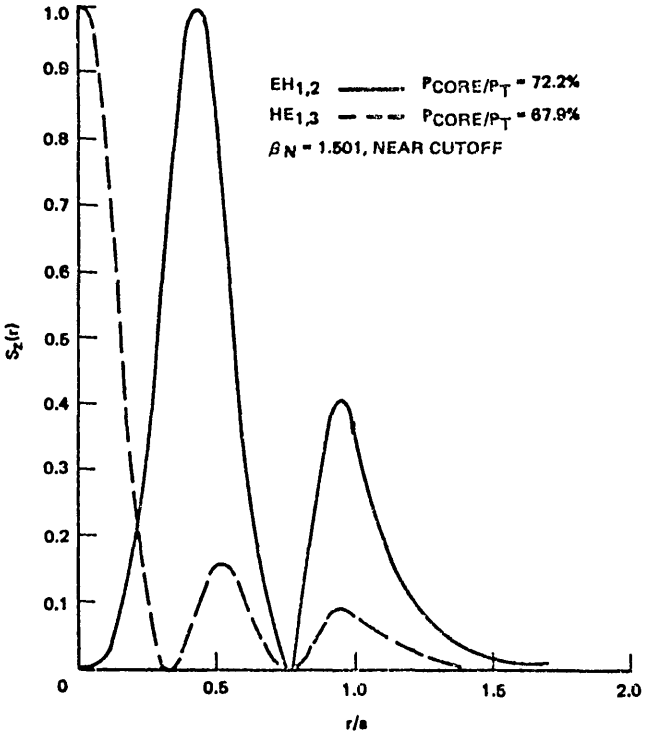

Fig. 9. Poynting flux characteristics of $EH_{1,2}HE_{1,3}$ modes. Fiber profile is homogeneous, $n_1 = 1.515$ and $n_2 = 1.500$.

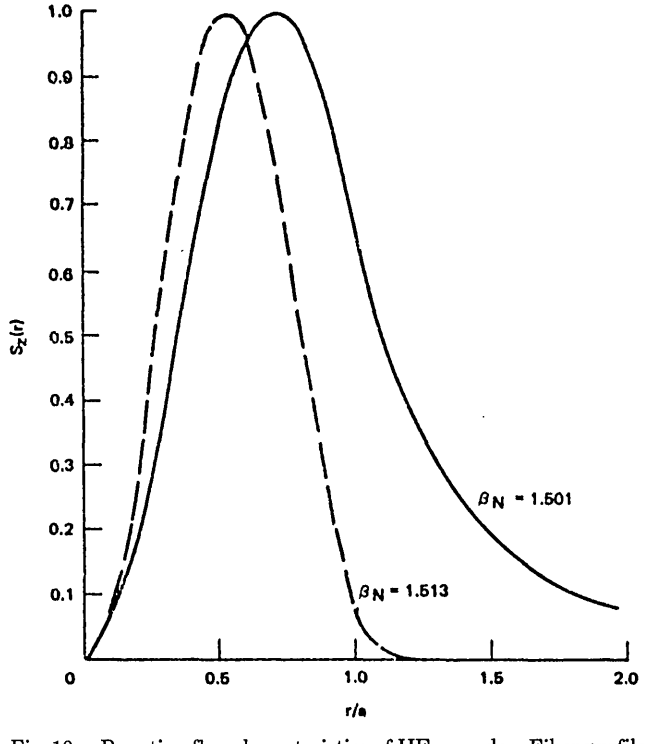

Fig. 10. Poynting flux characteristics of $HE_{2,1}$ mode. Fiber profile is homogeneous, $n_1 = 1.515$ and $n_2 = 1.500$.

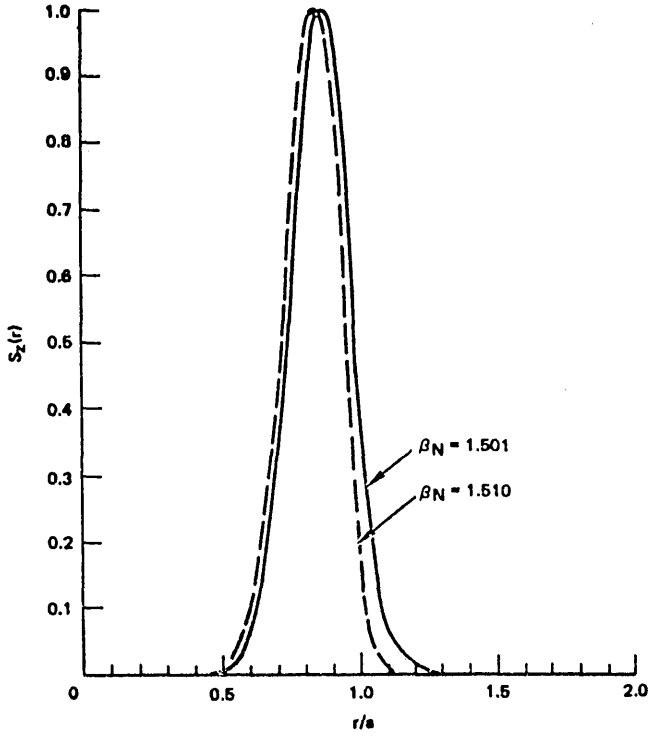

Fig. 11. Poynting flux characteristics of $HE_{10,1}$ mode. Fiber profile is homogeneous, $n_1 = 1.515$ and $n_2 = 1.500$.

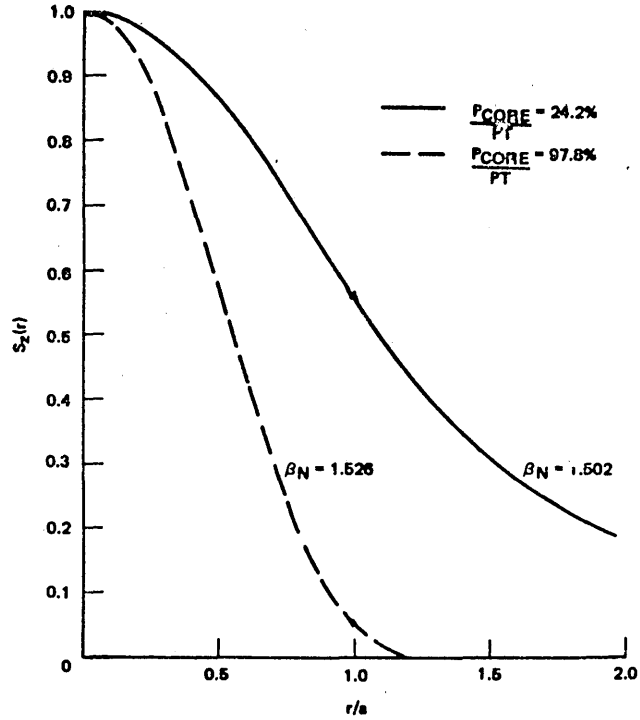

Fig. 12. Poynting flux characteristics of $HE_{1,1}$ mode. Fiber profile is homogeneous, $n_1 = 1.53$ and $n_2 = 1.500$.

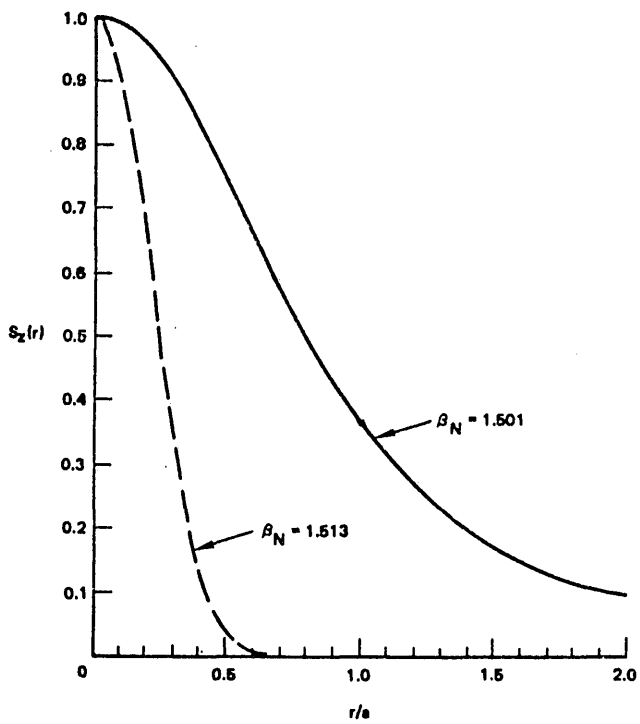

Fig. 13. Poynting flux characteristics of $HE_{1,1}$ mode. Fiber profile is parabolic (five layer), $n_{MAX} = 1.515$ and $n_2 = 1.500$.

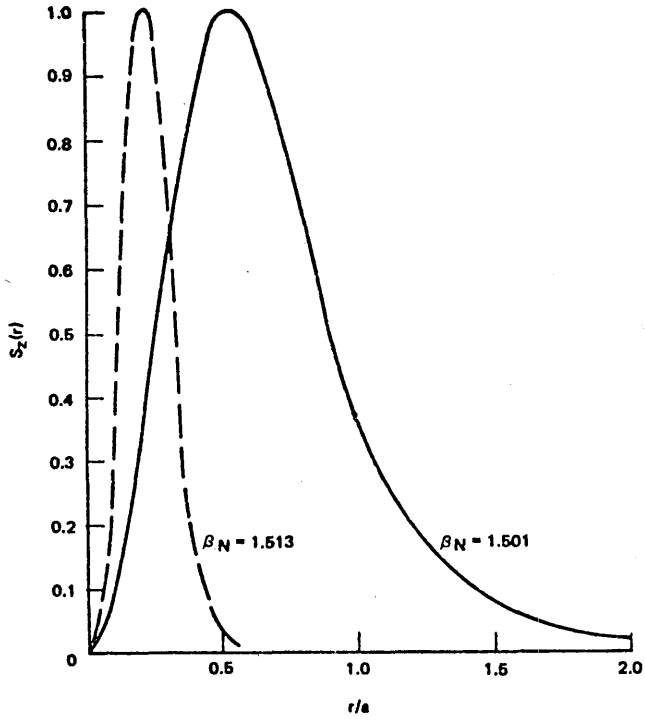

Fig. 14. Poynting flux characteristics of $HE_{2,1}$ mode. Fiber profile is parabolic (five layer), $n_{MAX} = 1.515$ and $n_2 = 1.500$.

core inhomogeneity; Figs. 15 and 16 show S_z for the doughnut profile. In these diagrams, the discontinuity is so slight that it is difficult to detect on the graphs; this is just what one would expect if the medium were continuously inhomogeneous.

The interesting feature of the inhomogeneous core guides is that the Poynting flux concentrates around the region of highest refractive index as the frequency is increased. In the case of the doughnut profiles at far above cutoff, the middle core region takes on the behavior of a slab guide where the peak refractive index serves as the core, and the layers inside and outside appear as the equivalent of a slab with upper and lower cladding regions.

Finally, a comparison was made between the homogeneous core and the parabolic core fiber with respect to radius and field confinement when used in a single mode application; the basis for the comparison was the $HE_{1,1}$ mode operated at $\beta_N = 1.507$, where $n_1 = 1.515$ and $n_2 = 1.500$. Figure 17 shows a rescaled parabolic core dispersion curve superimposed upon the homogeneous core $HE_{1,1}$ dispersion curve. The parabolic core fiber has a radius that is 1.66 times larger than the homogeneous core fiber. This is significant since it lends itself to improved launching efficiency and easier splicing between fibers. Figure 18 shows that the relative field confinement of the $r = 1.66a$ parabolic profile

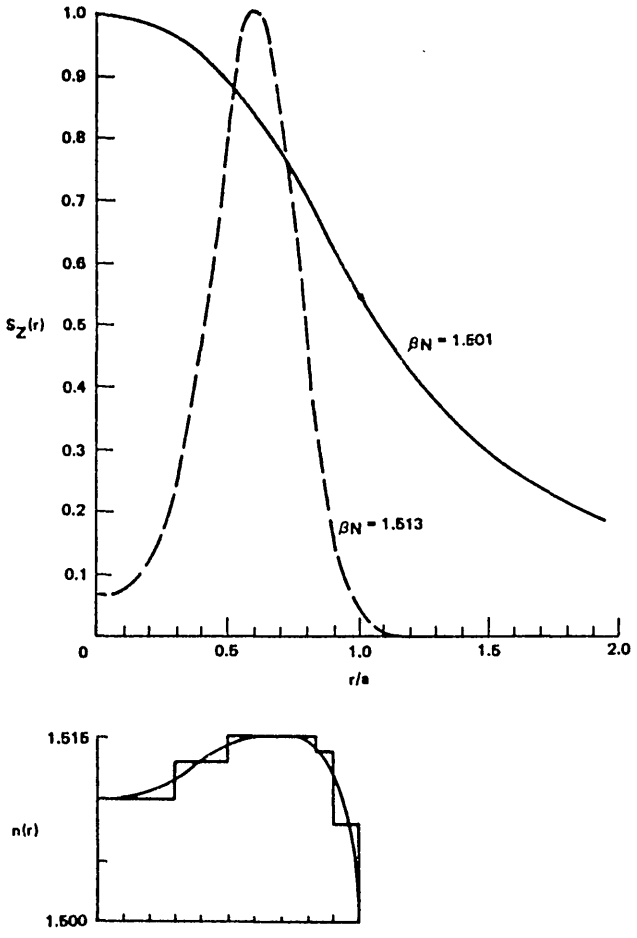

Fig. 15. Poynting flux characteristics of $HE_{1,1}$ mode. Fiber profile is doughnut (five layer), $n_{MAX} = 1.515$ and $n_2 = 1.500$.

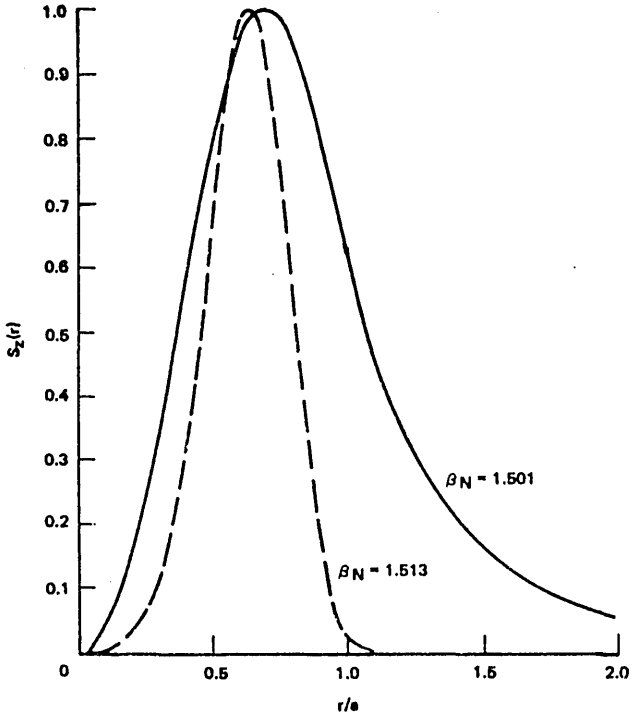

Fig. 16. Poynting flux characteristics of $HE_{2,1}$ mode. Fiber profile is doughnut (five layer), $n_{MAX} = 1.515$ and $n_2 = 1.500$.

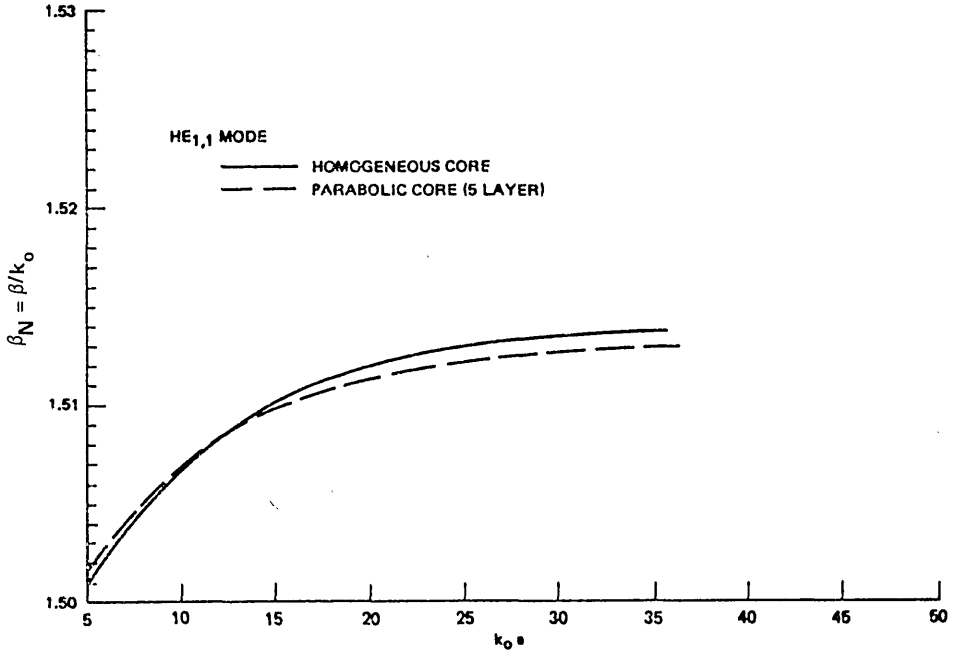

Fig. 17. Comparison of dispersion curves for homogeneous parabolic (five-layer) refractive-index profile fibers. Radius of parabolic core fiber is 1.66 times larger than homogeneous core radius.

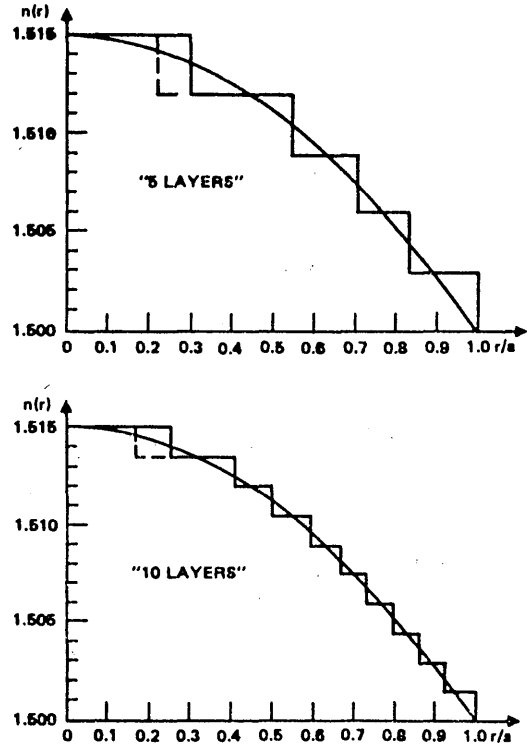

Fig. 18. Comparison of Poynting flux characteristics for homogeneous and parabolic (five-layer) core fibers. Radius of parabolic core fiber is 1.66 times larger than homogeneous core radius.

guide matches very well to a step profile guide of radius $r = a$.

In terms of dispersion, the refractive index profile has a pronounced effect on the guide dispersion characteristic. Of the profiles studied, the parabolic profile guide demonstrates the least dispersion. The factors that minimize pulse distortion in parabolic profile guide can be deduced from the generated dispersion curves. When one compares parabolic profile guide with step profile guide, the important differences are that for a parabolic profile guide (1) each mode is much less dispersive, (2) many modes have degenerate dispersion curves, and (3) for any given core size a and index difference Δn, the total number of propagating modes has been reduced, and these modes are mostly degenerate.

In terms of field confinement, the parabolic profile guide has a desirable property: when operating at single mode the parabolic profile guide with a core radius 1.66 times larger than a step profile guide has the same spot size as that of a step profile guide. This comparison was made on the basis that both guides are operating at the same frequency and wavenumber ($\beta_N = 1.507$, where $1.500 < \beta_N < 1.515$). If one connected the two guides with mismatched core sizes, one may expect efficient transfer of energy at the junction since the spot sizes, frequency, and wavenumbers all match. And finally, a comparison of the guide dispersions when operated under the above conditions indicates that the parabolic guide is still less dispersive than the step guide.

The doughnut profile guide was also studied in terms of dispersion and field confinement. The dispersion characteristics are intermediate to a step and parabolic profile guide, and the modes are not fully degenerate although the dispersion curves do show movement toward degeneracy. Hence, one would expect that multimode pulse distortion would also be intermediate to the other two types of guide. The doughnut guide has interesting focusing properties that confirm one's geometrical optics model of doughnut guidance. Even the fundamental $HE_{1,1}$ mode at high frequencies focuses onto the high index region as if the high index region were a slab guide. Thus, the doughnut guide has interesting possibilities as a transition from fiber to slab guide and an n-port power divider. For instance, one could join fiber of any profile to doughnut profile guide. Then, allow the doughnut guide to become very multimode by an increase in its diameter. When sufficiently multimode, the doughnut profile guide high-index region can be divided into azimuthal segments, each segment corresponding to a slab waveguide. The azimuthal segments can correspond to n-ports of a power divider with equal or unequal division.

And finally, it is interesting to note some general properties of fiber power flux density S_z. First, to evaluate $S_z(r)$, one must use accurate values for ω-β solutions; otherwise, large errors in S_z occur at the layer boundaries. Second, near cutoff, the percentage of power carried in the core vs that in the cladding does not approach zero for all modes; for instance, the $HE_{1,3}$ mode carries 69% of the power in the core even near cutoff. Third, far above cutoff, almost all the power is carried in the core, which confirms one's geometrical

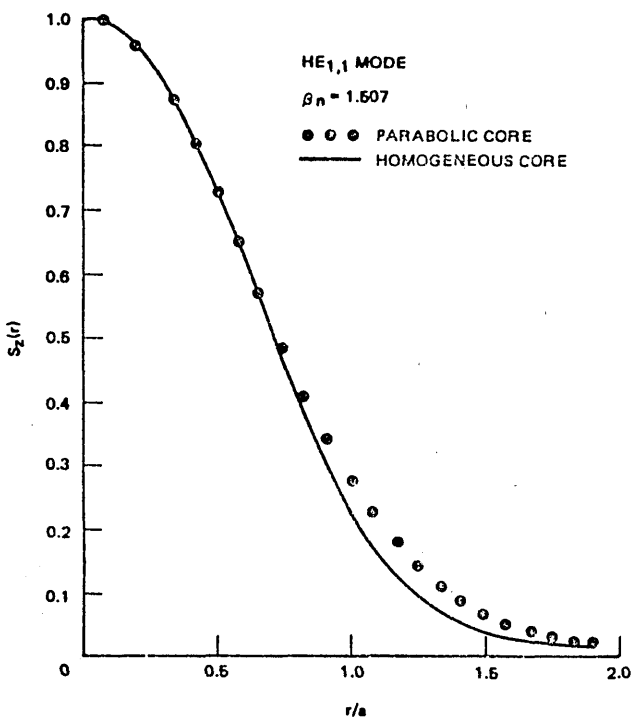

Fig. 19. Staircase approximations of parabolic refractive-index profile.

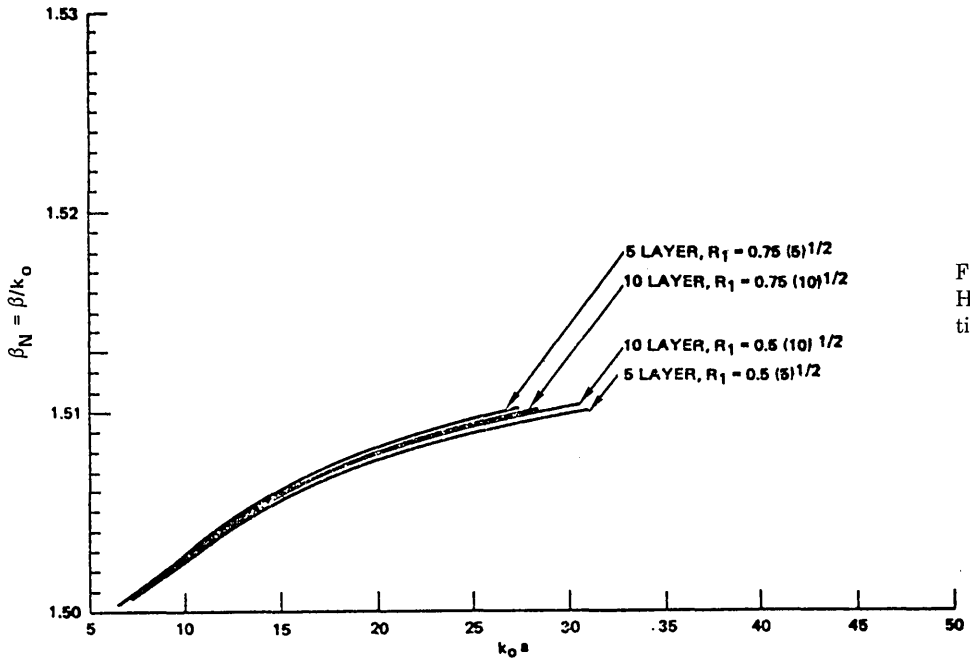

Fig. 20. Dispersion curves for $HE_{1,1}$ mode of parabolic refractive-index profile fiber approximated by five and ten layers.

Table I. Illustration of Error in $S_z(r)$ due to Error in $(\beta_N, k_o a)$ and P

β_N	$k_o a$	$\Delta k_o a$ Error	$S_z(r=a^-)$	$S_z(r=a^+)$	P
1.501	5.13593	0.0	.54888	.54438	-.99886
		0.5	.47937	.68664	-.996*
		1.0	.41087	.82311	-.996*
1.507	10.19825	0.0	.21555	.21770	-.99399
		0.5	.17623	.22763	-.996*
		1.0	.14052	.23554	-.996*
1.513	26.13023	0.0	.04209	.04231	-.99376
		0.5	.03343	.04215	-.996*
		1.0	.02581	.04171	-.996*

* P was fixed at -.996

Fiber Parameters: Homogeneous core, $n_1 = 1.515$, $n_2 = 1.500$

Dispersion Curve: $HE_{1,1}$ mode

optics model of fiber. And fourth, for a given mode and fiber profile, there is a relationship between R_β,

$$R_\beta = \frac{\beta_N - n_2}{n_1 - n_2}\ ;\ n_2 < \beta_N < n_1,$$

and the percentage of power carried in the core region that is independent of Δn. For example, the $HE_{1,1}$ mode operated at $R_\beta = 0.0666$ has 24.2% the power in the core whether Δn is 1% or 2%.

It may be worthwhile to mention that to obtain the pulse dispersion characteristics of an optical fiber, the group velocities of various modes must be computed. Detailed discussion of this important pulse dispersion problem for an inhomogeneous fiber will be given in another paper that is under preparation.

IV. Discussion of Computational Problems

In the study of the parabolic profile, the question arises: how many layers of stratification are needed, and how should they be distributed? Figure 19 shows the distributions that were selected to determine an answer. Figure 20 demonstrates the results. Clearly, the more layers of stratification one uses, the better the accuracy. On the other hand, as the number of layers is increased, the computer cost increases faster than linearly. Hence, five layers have been used to demonstrate the dispersion characteristics in terms of a reasonable compromise between accuracy and cost. The accuracy could be improved by the use of an unequal distribution of the stratification, that is, use large increments where the profile is flat and small increments where the profile is steep. Excellent accuracy could be achieved with ten layers as shown by Fig. 20 wherein ten layer stratification was relatively insensitive to a minor shift in a layer boundary location. However, the ten layer solutions were three times costlier to obtain than the five layer solutions. On the other hand, a four layer stratification showed a significantly different dispersion characteristic than did the five layer model. Hence five layer stratification was selected as the minimal number of layers that would achieve respectable accuracy at the lowest possible cost.

The cost associated with the use of more layers can be reduced by a decrease in the size of the search performed in $(\beta_N, k_0 a)$ space. This can be achieved by the definition of a small search neighborhood around the five layer $(\beta_N, k_0 a)$ solution.

Besides the cost of additional layers, further layering of the profile causes other computational problems. For any propagating mode, β_N is always takes on a value $n_i \leq \beta_N \leq n_{i+1}$. As the number of layers is increased, $\beta_N \simeq n_i$ or $\beta_N \simeq n_{i+1}$. Whenever this occurs, the radial wavenumber in the n_i region is approximately zero. This causes a computational problem in evaluation of the Bessel functions for the n_i region. However, this can be overcome through the use of small argument Bessel functions.

The computation of S_z is quite an involved process; in view of this, an investigation was undertaken to determine if one could easily generate S_z plots by the use of approximate values of $(\beta_N, k_0 a)$ such as could be taken from a dispersion diagram and by taking advantage of the properties of P (for HE modes, $P \simeq -1$, for EH modes, $P \simeq +1$). The value P is defined as follows: $P = [(\omega\mu)/\beta][(H_z)/(E_z)]$. The study of a homogeneous core $S_z(r)$ equation indicated that accurate values of P and $(\beta_N, k_0 a)$ are required; otherwise, erroneously large discontinuities in $S_z(r)$ occur at $r = a$. The results are summarized in Table I.

This work was supported in part by the U.S. Office of Naval Research.

References

1. J. G. Dil and H. Blok, Opto-electronics **5**, 415 (1973); M. O. Vassell, Opto-electronics **6**, 271 (1974).
2. G. L. Yip and Y. H. Ahmex, in *Proc. URSI Symposium of Electromagnetic Wave Theory* (1974), p. 272.
3. P. J. B. Clarricoats and K. B. Chan, Electron. Lett. **6**, 694 (1970).

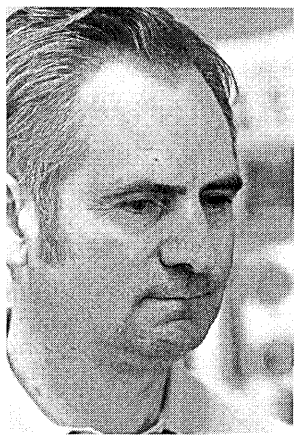

Helmut K. V. Lotsch of Springer-Verlag
Photo: W. J. Tomlinson, Bell Laboratories